Magneto-Optical Properties of Iron Oxide Nanoparticles for Use in Medical Imaging

Kathleen Oolman[1]

Subash Kattel[1], Katherine P. Rice[2], William D. Rice[1]

[1]University of Wyoming, Laramie, WY 82071

[2]National Institute of Standards and Technology, Boulder, CO 80305

Abstract

Due to their non-toxic and magnetic nature, magnetite iron oxide (Fe_3O_4) nanoparticles have potential uses in biomedical applications such as for magnetic resonance (MR) contrast agents. In this work, the physical properties of rare-earth element doped (Tb and Eu) and undoped iron oxide nanoparticles are optically investigated. Absorption and photoluminescence (PL) from doped and undoped iron oxide nanoparticles in solution show a well-defined excitonic absorption and weak PL. When the nanoparticles are drop cast into thin films, the absorption spectra remains unchanged while the PL disappear, suggesting the thin film creates non-radiative relaxation pathways. Low-temperature absorption measurements are also performed on the undoped iron oxide thin films.

To further characterize optical properties of Fe_3O_4 nanoparticles and other materials, a spectrofluorometer is reconstructed for absorption and PL measurements. This consists of rewiring and controlling three motors, to adjust the slit width and rotate a double monochromator, a photo-gate, and reflective sensor using a micro-controller interface.

1 Introduction

1.1 Rare-Earth Doped Iron Oxide Nanoparticles

Due to their non-toxic and magnetic nature, magnetite iron oxide (Fe_3O_4) nanoparticles have potential uses in biomedical applications, such as for magnetic resonance imaging (MRI) contrast agents. Magnetite has an inverse spinel crystal structure, with Fe^{3+} filling the tetrahedral lattice positions, and Fe^{2+} and Fe^{3+} in the octahedral lattice positions[1]. The magnetic moments of the iron in the tetrahedral positions are oriented anti-parallel to the magnetic moments of the octahedral iron atoms[1].

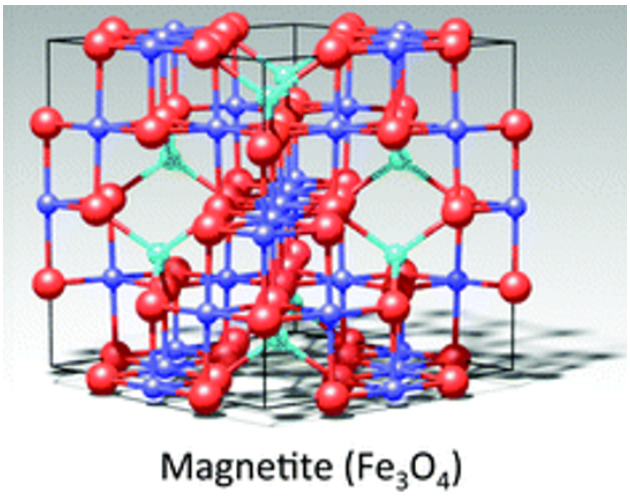

Figure 1: Structure of magnetite iron oxide, (Fe_3O_4), where the red atoms are oxygen, teal atoms are tetrahedral iron, and blue are octahedral iron[2].

Nanoparticles (NPs) have recently been found to have a use as magnetic resonance (MR) contrast agents[3]. The NPs are injected into the desired tissue and either reduce spin-lattice relaxation time (T_1), which lightens the image where the NPs reside, or reduce spin-spin relaxation time (T_2), which darkens the image. Magnetite iron oxide nanoparticles, called superparamagnetic iron oxide (SPIO) NPs are currently used as T_2 MR contrast agents ranging in size from 10 nm to 3.5 μm in diameter[4]. Smaller diameter NPs are desirable to enable the targeting of smaller organs, such as lymph nodes, as well as to provide better MR image contrast. Smaller NPs provide longer circulation times, which increase tissue

contrast[3][4]. Smaller SPIO nanoparticles also have the potential to be used as T_1 contrasting agents.

In addition to MR contrasting agents, NPs could be used for optical imaging. For example, rare-earth dopants could be used to enhance the optical properties of magnetite iron oxide NPs, due to their large spin and optical moments, for use in optical imaging[5]. Since optical moments of rare-earth metal dopants lie in the f-orbitals, these moments remain as the dopants are put into a lattice. Additionally, rare-earth metal dopants may also improve the magnetic properties and reduce the oxidation of iron oxide NPs[6]. Therefore, rare-earth metal doped iron oxide NPs could be used as a dual purpose MR imaging and optical imaging agent, for non-invasive soft tissue imaging.

Specifically, terbium (Tb^{3+}) and europium (Eu^{3+}) can replace Fe^{3+} atoms in the octahedral crystal lattice structure of magnetite iron oxide NPs. In doing so, the crystal shape changes from spherical to cubic particles[5]. Also, rare-earth metals tend to cluster on the outside of the NP. This is due to the large mismatch in size between the iron and rare-earth metal atoms; for example, iron has an ionic radii of 78.5pm, while terbium has an ionic radii of 106.3pm.

Rare-earth metal dopants in NPs are rare at this point, and the optical and magnetic properties of rare-earth metals dopants in NPs are not well understood. Therefore, the optical properties of magnetite iron oxide NPs along with Tb- and Eu-doped iron oxide NPs are studied. Both the doped and undoped NPs had a diameter of about 5nm[5], and are optically characterized using absorption and photoluminescence.

1.2 Nanoparticles

Magnetite iron oxide is a semiconductor material. The energy diagram of a semiconductor consists of a full, electron filled valence band, a band gap, where electrons cannot reside, and a conduction band empty of electrons. A semiconductor material can absorb a photon, which excites an electron from the valence band to the conduction band. This creates a negative charged electron in the conduction band, and a positive hole in the valence band. This optically generated electron-hole pair is coulombically bound, much like a hydrogen atom. Like a hydrogen atom, the electron-hole pair consists of a single negative charge bound to a

single positive charge, except the positive hole is much lighter than a proton of a hydrogen nucleus. The electron-hole pair is a bosonic entity is called an exciton, and dominates the optical properties of semiconducting NPs.

As the size of the semiconductor decreases in size to a diameter smaller than the Bohr diameter of the exciton, the semiconductor shows what is known as the quantum size effect[7]. This effect is the quantization of optical transitions, such as absorption and photoluminescence (PL), in the valence and conduction band, which is similar to atomic transitions. These optical transitions are dependent on the size of the particle. Therefore, it is useful to approximate the energy levels by the particle-in-a-sphere model. In this model, the potential energy well of the particle is approximated as

$$V(r) = \begin{cases} 0 & r < a \\ \infty & r > a \end{cases}$$

where a is the radius of the particle. Solving the Schrödinger equation using this potential yields the energy of the particle as

$$E_{n,l} = \frac{\hbar^2 \alpha_{n,l}^2}{2m_0 a^2}$$

which shows the dependence of the energy levels on the size of the particle.

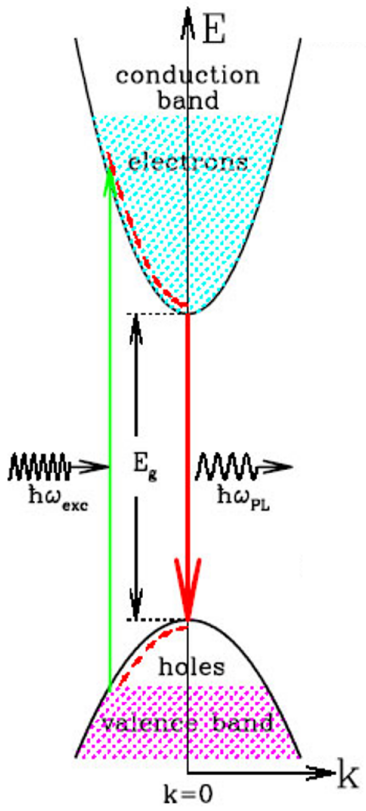

Figure 2: Simple diagram of energy versus momentum band structure of a semiconductor. The absorption process is shown with the green arrow, and PL process shown with the red arrow[8].

Absorption and photoluminescence are two techniques used to optically characterize semiconductor nanoparticles. Absorption is the process of exciting an electron from the valence band to the conduction band. To measure absorption, a beam of light of a known wavelength is passed through the NP sample, and the exciting light measured. If a certain wavelength of light matches the difference between two energy levels, the light will be absorbed and not pass through the sample. Therefore, the measured light is actually the transmittance of light through the sample. The transmittance, T, can be converted to absorbance, A, with the equation

$$A = -log_{10}\left(\frac{T_S - T_D}{T_R - T_D}\right)$$

where T_S is the sample, T_R is a reference sample, and T_D is "dark" or the transmittance

without any interference.

Photoluminescence (PL) is the emission of light as the electron loses energy to move from the conduction band back to the valence band. The emitted light has the same energy as the energy lost by the electron, by the conservation of energy. The electron is excited to the conduction band by a excitation light source, such as a laser. There resides a positively charged absence of the electron in the valence band, called the hole. As shown in figure 2, the electron-hole pair may have a non-zero momentum. Both the electron and the hole will release energy and momentum through phonon emission, to reach a point where they have lost all their momentum, at $k = 0$. Then, radiative recombination of the electron and hole produces a photon emission called photoluminescence.

1.3 Varshni Shift in Temperature-Dependent Optical Transitions

The band gap energy of a semiconductor is a parameter of the material. However, the band gap energy can change slightly in energy with temperature. This results in an excitonic absorption peak or PL peak that shifts in energy with temperature, known as the Varshni shift[9]. The band gap energy as a function of temperature (T) can be described as

$$E_g(T) = E_0 - \frac{\alpha T^2}{T + \beta}$$

where E_0 is the band gap energy at 0 K, and α and β are constants dependent on the material. The Varshni shift is seen due to the existence of thermal energy at higher temperatures. Thermal energy induces the shift in conduction band and valence band positions, with temperature-dependent dilation of the lattice and electron lattice interaction[9].

1.4 X-ray Diffraction

X-ray diffraction (XRD) is the process of scattering x-ray electromagnetic light off atoms in a crystal. The atoms are oriented in a regular array, which acts similarly to a diffraction grating. As incident light reflects off the atoms, it interferes constructively and deconstructively. This creates light spots where the incident light interferes constructively, and dark spots where the interference is completely deconstructive. The location of the bright constructive interference follows Bragg's Law,

$$2d\sin\theta = m\lambda$$

where d is the atomic spacing, θ is the angle between incident light and the crystal surface, m is the order, and λ is the incident wavelength of light[10].

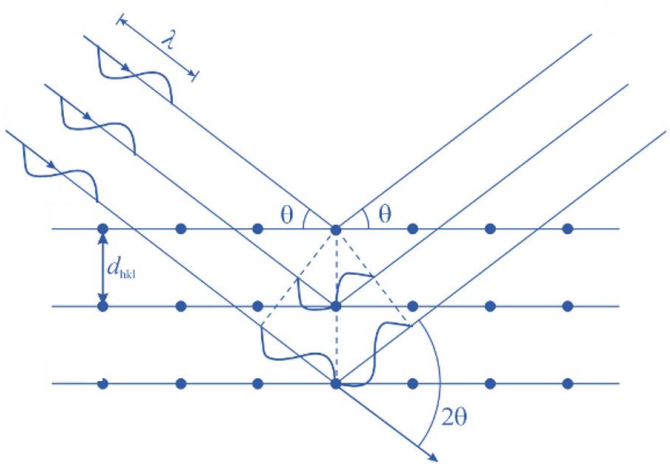

Figure 3: Diagram of Bragg's Law. The incident x-ray light strikes the lattice and reflects off the atoms to create interference pattern[11].

From Bragg's Law, it follows that the incident wavelength of light cannot be much greater than the atomic spacing of the lattice. If the wavelength is longer than the atomic spacing, only the zeroth order (m=0) maximum is possible, which gives little information on the crystal lattice structure. Since the typical crystal atomic lattice spacing is on the order of angstroms Å, (10^{-10} m), x-rays, with a wavelengths of about 0.6 Å to 125 Å, are ideal for the incident light source for XRD measurements.

To characterize lattice structure in a solid, XRD can be used. Iron oxide exists in three major forms, magnetite (Fe_3O_4), maghemite (γ-Fe_20_3), and wüstite ($Fe_{1+x}0$)[2]. These three types change in crystal structure, which may affect the optical properties. XRD could be used to determine which type of iron oxide NPs are being studied. The different crystalline structure of each type will result in a unique XRD pattern.

1.5 Lock-in Amplifier

Lock-in amplifiers allow for the detection of low-intensity light signal that may be otherwise lost in noise. The lock-in amplifier uses a technique called phase-sensitive detection[12]. This technique picks out a signal with the desired frequency and phase out of a signal with multiple frequencies. The lock-in amplifier has two inputs, one from the signal with the noise, and one as a reference, where the reference and signal oscillate at the same frequency and phase. For light beams, this can be accomplished with the use of a mechanical chopper. The chopper rotates at a known velocity, which causes the light beam intensity to modulate with a known frequency. The reference signal is then set to oscillate at this frequency as an square wave. The reference signal is taken as a square wave from the chopper motor drive. It is often desired that the oscillation frequency is a prime number, and not near to a multiple of 60 Hz. This minimizes the possibility of electronic pick-up from the grid, which normally has a frequency of 60 Hz, from masking and mixing with the signal. In this work, an oscillation frequency of 137 Hz was used.

To detect the light signal from the noise, the lock-in amplifier compares the light signal to the reference. The reference signal is approximated as a sinusoid, $A\sin(\omega_m t + \phi_0)$, with at the fundamental frequency, $f = \frac{\omega}{2\pi}$. The sinusoid is multiplied by the light signal, which can be decomposed into a sum of sinusoidal waves as $\sum_{n=1}^{\infty} A_n \sin(\omega_n t + \phi_n)$. This sum is integrated to get the modified signal, I_{mod} such that

$$I_{mod} = \int A\sin(\omega_m t + \phi_0) \sum_{n=1}^{\infty} A_n \sin(\omega_n t + \phi_n) dt$$

The sine functions are always orthogonal, except in the case where $m = n$. Thus, all the sinusoidal light waves with a frequency different than the target frequency are eliminated, leaving only the desired light signal. This chooses and amplifies the desired signal, with the same frequency as the reference signal, while filtering out any other signal which may be present.

2 Methods

2.1 Absorption

The absorption measurements of magnetite NPs in solution and in thin films were measured by a Cary UV-Vis-IR spectrometer at room temperature. The thin film absorption measurements were also measured with a system built on the optical table in lab which can be used at low-temperatures and in a magnetic field. The optical table system consisted of a 150 W xenon lamp white light source connected to a monochromator. As the light left the monochromator, it passed through a mechanical chopper connected to a lock-in amplifier. The lock-in amplifier allowed light from the source to be differentiated from ambient room light as discussed previously. After passing through the sample, the light was collected with a silicon photodiode which measured the transmittance of light through the sample. A reference measurement was performed using a blank glass cover slip.

2.2 Photoluminescence

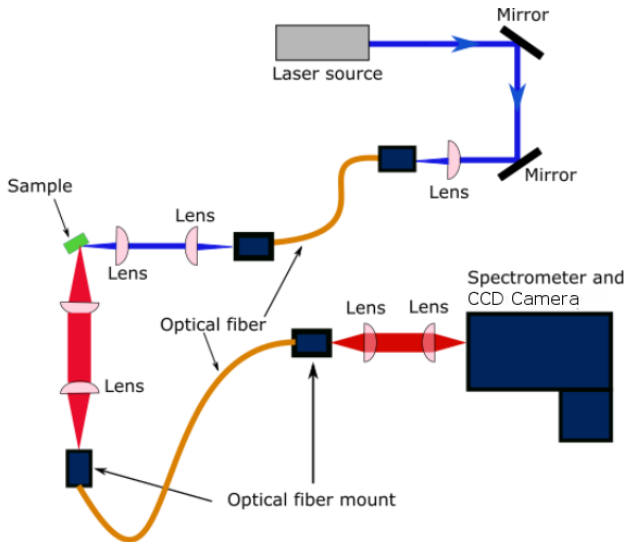

Figure 4: Experimental setup of PL measurements with 405 nm diode laser excitation source.

Photoluminescence of the magnetite NPs was measured in solution and in thin films and compared with the PL of a reference blank glass cover slip. The excitons were excited

with a 405 nm wavelength diode laser with a power of 1.3 mW as shown in figure 4. The PL was collected and passed through a monochromator and detected by a Pylon LN_2-cooled CCD light detector. A 440nm cut off filter was placed between the sample and detector to filter out any light from the excitation source.

2.3 Thin Film Preparation

In order to measure low-temperature properties of magnetite iron oxide NPs, the NPs had to be in thin films instead of in solution. Thin film preparation was tested using undoped magnetite iron oxide NPs in hexanes. The films were created by three methods, spin coating, drop casting, and modified drop casting.

For the spin coating method, a single drop of NP solution was dropped onto a glass cover slip rotating at a constant speed. Each trial had a unique speed in a range of 500-1200 revolutions per minute. The cover slip was allowed to rotate at the constant speed until the hexane isomer solution had completely evaporated.

For the drop cast method, the NP solution was pipetted and dropped onto a glass cover slip. The solution was dropped two drops at a time, and the hexanes were allowed to evaporate without disturbance. This process was repeated until about eight drops of nanoparticle solution was deposited on the cover slip.

Finally, the drop cast method was modified to create a more uniform thin film. In this method, the NP solution was dropped onto a glass cover slip in the same fashion as the drop cast. However, as the solution was drying, the NP solution on the cover slip was stirred with the tip of a glass pipette. A similar method was also used with the use of the sharpened tip of a wooden applicator stick instead of a glass pipette tip. With the wooden applicator stick, the hexane isomer solution was allowed to mostly evaporate but the NP were still wet before the NP solution was stirred.

2.4 Low-Temperature Absorption

The transmittance of the undoped thin film was measured at low temperature. This was accomplished by using the optical absorption system described above and shown in figure 5. Instead of placing the sample on the bench, the sample was placed inside of a cryogen-free

cryostat, and the light beam allowed to pass through the cryostat and sample. A reference measurement was again performed by using a blank glass cover slip.

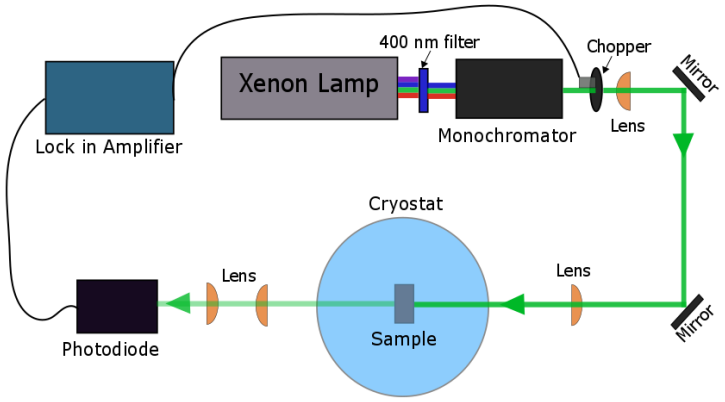

Figure 5: Experimental setup of low-temperature absorption measurements.

2.5 Spectrofluorometer Reconstruction

A spectrofluorometer was reconstructed for absorption and PL measurements. The spectrofluorometer consisted of two Czerny-Turner monochromators. The dual monochromators allowed for narrow frequency light selection from a white light source. The electronics for the spectrofluoremeter were outdated, but the mechanical hardware was still functional. New electronics and computer were needed to control two slit motors, to control the input and exit slit, a rotational motor, to control the two Czerny-Turner monchromators, a photo gate, and reflector sensor.

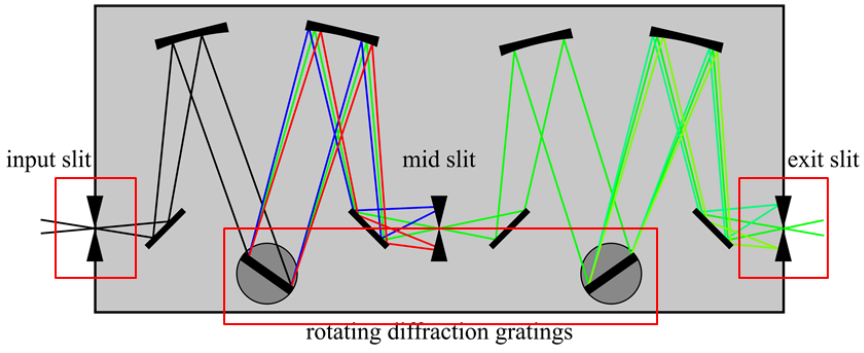

Figure 6: Spectrofluoremeter with two Czerny-Turner monochromators diagram. The motors to be controlled are shown in the red boxes.

3 Results and Analysis

3.1 Absorption

The absorption of the magnetite iron oxide NPs was measured first in the Cary spectrometer, and second in the optical system set up in lab. This was done to test the accuracy of the optical system. As seen in figure 7, the absorption between both systems matched with an absorption peak seen around 2.6 eV. The roughness of the optical table absorption measurement resulted from unresolved xenon plasma lines. This proved that the optical system could be used for all absorption measurements.

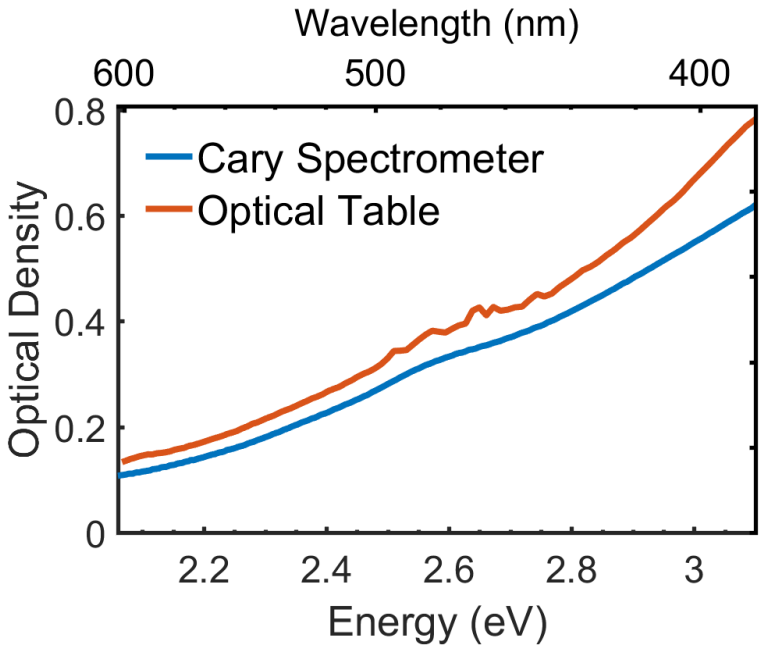

Figure 7: The absorption spectrum of magnetite iron oxide NPs measured with the Cary spectrometer and optical table system.

This absorption spectrum shows the existence of an exciton formation with energy around 2.6 eV. This absorption peak corresponds to the excitation of an electron from the valence band to the conduction band formed by the 2p orbital of oxygen, and 4s orbital of the octahedral iron[13].

3.2 Absorption and Photoluminescence of Magnetite NPs in Solution

Excitonic absorption was found of magnetite NPs in solution at an energy of 2.6 eV shown in figure 8. The absorption was measured with the Cary Spectrometer. The PL of magnetite NPs in solution was also measured. The solution was excited at 3.06 eV (405 nm) with a power of 1.3 mW on the sample. The magnetite NPs in solution showed a weak photoluminescence around 2.5 eV (496 nm). The shift in absorption and PL peaks is from the relaxation of the electron and hole to where $k = 0$, or there is no momentum. This process also released energy in phonon emission, which causes the PL peak to be at a lower energy than the absorption peak.

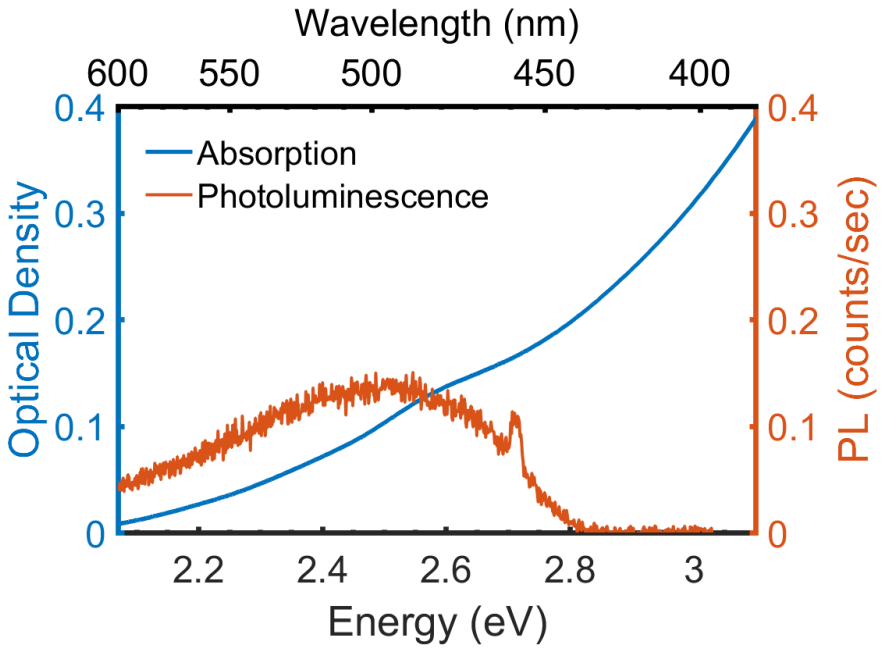

Figure 8: Absorption and photoluminescence of magnetite NPs in solution.

The PL found for the NPs was congruent with results found in literature. Sadat et al. found PL peak of magnetite NPs to exist between 500 nm to 600 nm, corresponding to an energy of 2.07 eV to 2.48 eV[13]. The shift in PL peak was accounted for with the NP size. As previously mentioned, band gap energy depends on the size of NP, and can be modeled as a particle-in-a-sphere approach. This dependence showed that as the NP size decreases, the band gap energy increases, which shifted the PL peak to smaller wavelengths and higher

energy. In the study done by Sadat et al., the NP diameters ranged from 10 nm to over 100 nm, versus a diameter of 5 nm in this study, which caused the observed shift in PL peak.

3.3 Thin Film Preparation

The spin coating method of thin film preparation resulted in a uniform thin NP layer. However, this method lost a lot of material that was spun off the glass cover slip before the hexane could fully evaporate. This was undesirable when creating thin films for the Tb- and Eu-doped iron oxide samples, since the amount of doped NP solution is limited. The thin coating produced by the spin coating method also has few and largely spaced nanoparticles, which makes absorption and photoluminescence measurements weak.

The simple drop cast method produced a thicker layer of NPs. But, since hexane evaporated quickly, thick NP rings were formed. This method creates a non-uniform film of NPs, with rings of densely packed NPs and rings with no NPs. This makes optical measurements difficult since the concentration of nanoparticles changed over a small area. The localization of NPs becomes an even larger problem when placing the NP thin film in the cryostat, since placement control is difficult.

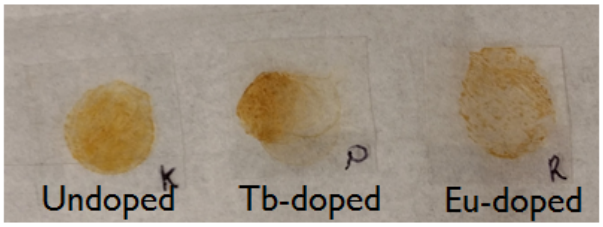

Figure 9: Results of thin film preparation with the modified drop cast method.

The modified drop cast method produced a relatively thicker, more uniform thin NP film. When the nanoparticle solution was stirred with the glass pipette tip, a more uniform film than the drop cast could be created, but the ringed pattern was still present. With the wooden applicator stick, a mostly uniform thin film could be created. This method proved to be the best method to create a thick, mostly uniform thin film. However, some inconsistencies in the thin film were still present. For this reason, the Tb- and Eu-doped magnetite NP thin films were made with the use of the wooden applicator stick method.

3.4 X-Ray Diffraction

To determine the structure of the magnetite NPs, x-ray diffraction measurements were attempted with undoped magnetite NP thin films. Two thin films of different thicknesses were used for x-ray diffraction measurements. The results for both tests were similar: no resolvable x-ray diffraction peaks were visible, as shown in figure 10 despite the sample being successfully measured previously. Rice et al. found an x-ray diffraction spectrum characteristic of magnetite iron oxide upon previous measurement[Rice]. The peak around 45° in Figure 10 was characteristic of the x-ray diffractometer. The shape around 25° was due to the glass cover slip.

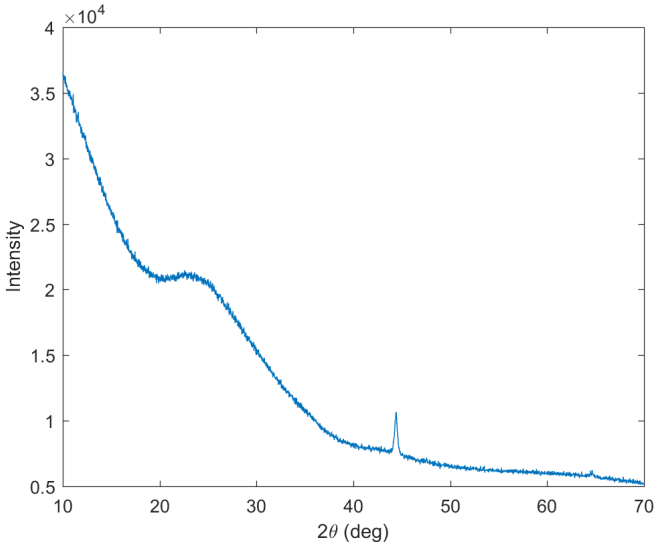

Figure 10: 2-theta x-ray diffraction spectrum of magnetite NP thin film. The 25° peak is due to the glass cover slip.

3.5 Absorption of Magnetite NP Thin Films

The optical properties of magnetite NP thin films were tested in the same method as the solution. This was done to determine if the optical properties changed in the process of creating a thin film. The absorption of the undoped magnetite NP thin films were measured using the Cary spectrometer and shown in figure 11. The excitonic absorption peak of the thin films were found to match the peak of the NPs in solution. From these measurements,

it was determined that the film-making procedure did not significantly alter the NP optical absorption. Typically, strain caused by film drying or immersion into a polymer matrix will shift the absorption features in NP films from their solution state.

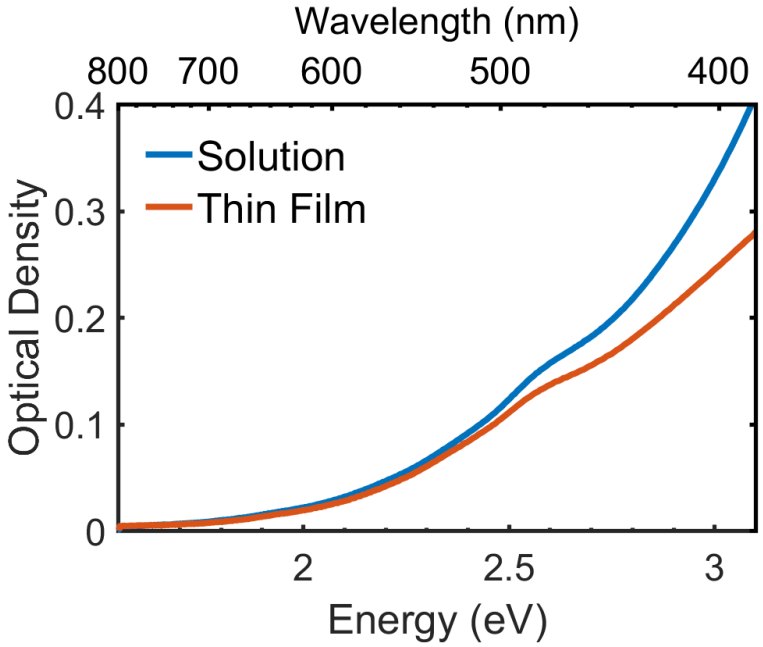

Figure 11: Absorption of magnetite NPs in solution and in thin film.

3.6 Photoluminescence of Magnetite NP Thin Films

Photoluminescence measurements were also taken of undoped magnetite NP thin films. The results are shown in figure 12, with PL of the magnetite NPs in solution PL shown in blue, and PL of the magnetite NPs thin films PL shown in red. Since there exists a large discrepancy in the the PL intensity and peak energy (about 0.5 eV PL peak shift), the PL of a blank glass cover slip was also measured and shown in yellow. These results show that the PL of the undoped magnetite NPs disappeared in the process of the thin film preparation.

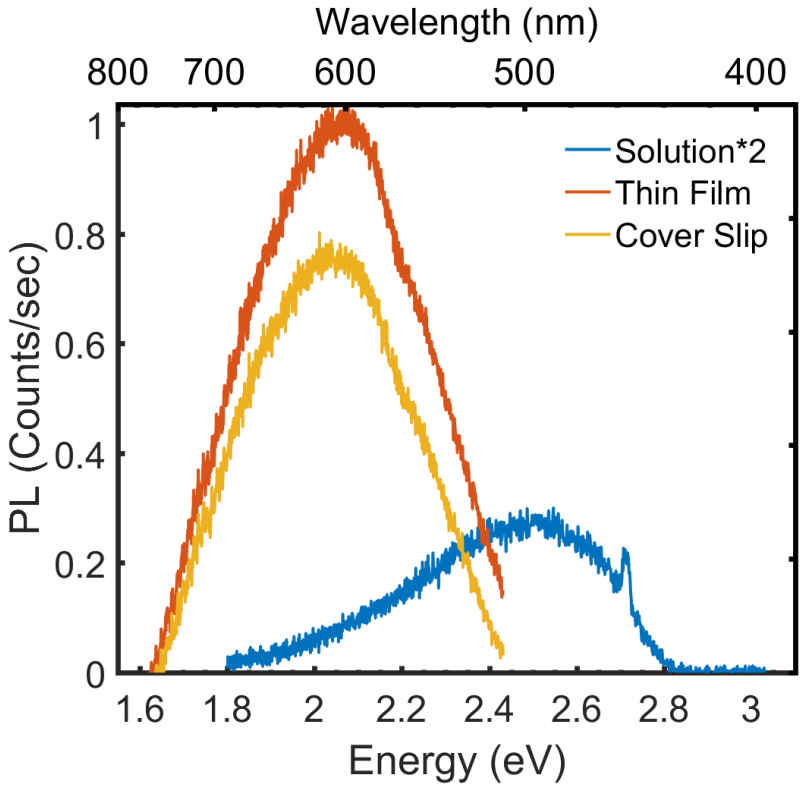

Figure 12: PL of magnetite NPs in solution and in a thin film. PL of the magnetite NPs is also compared with the PL of a glass cover slide. The NPs in a thin film do not show any measurable PL.

The PL of the glass cover slip could be dominating over any PL of the thin film sample. The PL of only the glass cover slide had a PL peak around 2.0 eV with an intensity of 0.8 counts per second. This was compared to the PL of the magnetite iron oxide NPs in solution, which had a PL peak at 2.5 eV with intensity of only about 0.1 counts per second. The thin film consisted of less NPs per volume than found in solution, so any PL of a NP thin film had a smaller intensity than NPs in solution. In this situation, this may have caused the the NP PL to nearly disappear. Since the PL of the magnetite NPs in solution was small to begin with, and a thin film will had even less PL intensity, so any PL from the magnetite NPs thin film could have been overshadowed by the PL of the glass.

Alternatively, the thin film creation could have caused non-radiative relaxation processes to dominate. A possible mechanism for non-radiative relaxation processes was shown in the paper published by Sadat et al.[13] The paper showed an energy band schematic of magnetite iron oxide NPs. This included an excitonic absorption of a photon in between the oxygen and the octahedral Fe^{3+} and Fe^{2+} atoms with an excitation energy of 3.04 eV. A radiative relaxation process had an emission energy of 2.2 eV, in agreement with the results found. An alternate non-radiative relaxation process was also shown. In this process, the exciton relaxes non-radiatively to an electron trap before an addition radiative relaxation with an energy of 1.8 eV. The PL peak of the magnetite iron oxide NPs thin film lay around 2.0 eV, which could correspond to this alternate non-radiative relaxation process shifted due to the change in NP diameter.

The relaxation time of semiconductors, τ, follows a rate equation, where

$$\frac{1}{\tau} = \frac{1}{\tau_R} + \frac{1}{\tau_{NR}}$$

where τ_R is the radiative recombination rate, and τ_{NR} is the non-radiative recombination rate. The thin film preparation could cause the recombination rates to change. In this process, if $\tau_{NR} << \tau_R$ then, $\tau \approx \tau_{NR}$, and the radiative recombination becomes unfavorable. Whether the magnetite iron oxide NPs thin film followed this non-radiative path was impossible to determine due to the definite PL of the glass cover slide located at the same energy.

3.7 Absorption at Low Temperature of Magnetite NP Thin Film

Since there was no observable PL of the magnetite NP thin film samples, only absorption measurements were taken at low temperature. Absorption measurements were taken at various temperatures ranging from 1.5 K to 300 K and shown in figure 13. A Varshni shift in absorption peak was expected with a change in temperature. However, the absorption peaks were unresolvable with the presence of plasma lines from the xenon lamp source, so no peak shift was observed. This was because the shift peak was expected to be small, and was lost in the xenon lamp plasma lines, which accounted for the roughness in the absorption peak seen between 2.5 eV and 2.8 eV. For an example of the size of a Varshni shift, a study done by Najar, Shafa, and Anjum, showed a Varshni shift of GaN nanowires at temperatures from

78 K to 273 K[14]. In this temperature range, the band gap energy changed 0.06 eV.

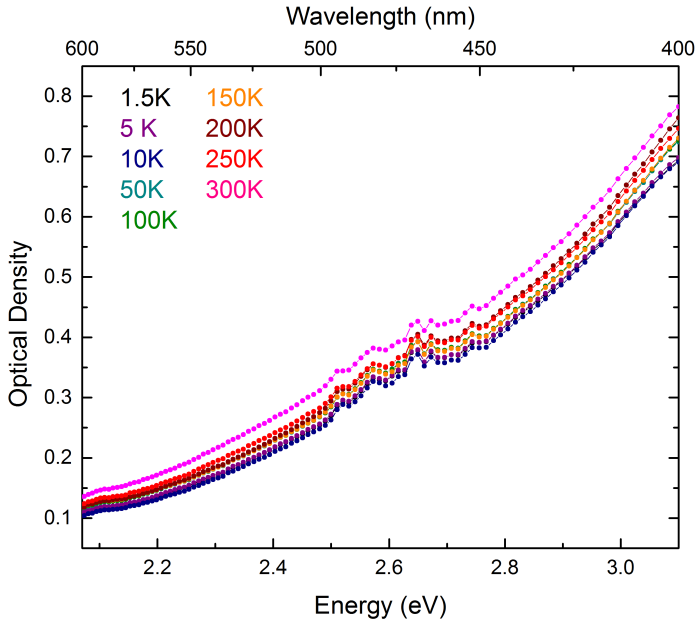

Figure 14: Absorption of magnetite NP thin films at various low temperatures. The presence of the xenon lamp plasma lines obstructed the expected shift with temperature.

While the absorption shift should should have been larger for the magnetite iron oxide NPs due to the lower temperatures reached in this study, the Varshni shift was still smaller than the resolution of the low-temperature absorption system. The resolution may be solved by measuring the reference directly following the sample measurement. This technique was not possible at the time of the study, so the magnetite NPs thin film sample measurements had to be taken on a separate day as the reference measurement. With a new cryostat sample stick, both the sample and reference could be placed in the cryostat simultaneously, which would allow for a reference measurement to directly follow the sample measurement. This would hopefully resolve the xenon lamp plasma lines, and a Varshni shift in the absorption peak will be observable.

3.8 Doped Magnetite NP Thin Film Absorption

The absorption of the Tb- and Eu-doped magnetite NP thin films were measured and compared with undoped magnetite NP thin films at room temperature. The results showed an excitonic absorption peak for each doped sample at the same energy as the undoped sample, so no significant shift in absorption peak is present at room temperature between the doped and undoped sample. The properties of the Tb-doped NPs are expected to change at lower temperatures and under the influence of a magnetic field, where the Tb spins begin to couple and polarize to the magnetite lattice[5]. Similar results are also expected for Eu-doped NPs.

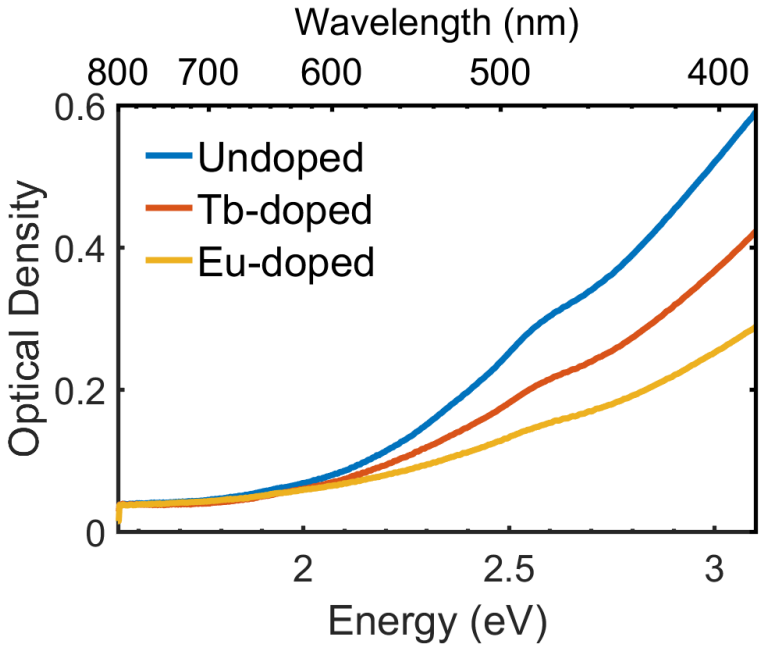

Figure 15: Absorption of undoped magnetite thin film compared with Tb-doped and Eu-doped magnetite thin films.

3.9 Spectrofluorometer Reconstruction

An Arduino Uno micro-controller was used to control the spectrofluorometer. The Arduino micro-controller was connected to LabView, to receive commands directly inputted on the computer interface. This allows for the Arduino micro-controller to receive updated instructions, such as a change in slit width, without the need to completely reload the program

onto the Arduino for every change. The two slit motors and monochromator motor were stepper motors, and controlled with the digital pins on the Aruduino Uno and programmed with the Arduino software's built-in stepper motor function. This enabled the motors to step forward or backwards any number of steps and at a given speed. The step size of these motors still needed to be calibrated. To calibrate the slit motor, a single-slit diffraction calibration would be used. A collimated laser beam of light would pass through the slit to create a diffraction pattern on the back wall. This diffraction pattern would be imaged with a CCD camera for analysis and the distance between bright fringes will be determined. Then, the slit motor would be commanded to increase the slit by one step. This would change the slit size, and thus, the distance between bright fringes. The size of the slit and change in slit size per step could then be calculated.

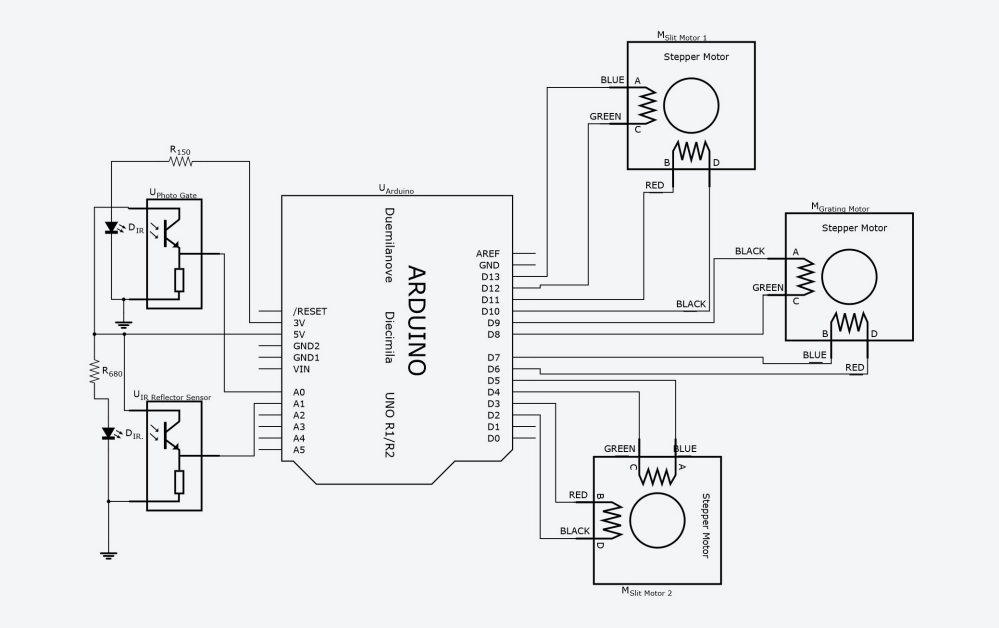

Figure 16: Circuit diagram of Arduino Uno micro-controller connected to two slit width motors, grating step motor, photo-gate sensor, and IR reflector sensor.

The analog pins of the Arduino Uno were used to control the photo-gate and reflector sensor, which were both connected to the monochromator motor. The photo-gate was used to determine how far the monochromators have rotated. It consisted of an infrared light emitting diode (LED) and infrared photo detector. As the monochromator motor moved,

it rotated a solid disk with a single hole punched in the edge. The infrared detector did not receive any light until the hole passed in front of the infrared LED light. This creates a changed in voltage across the infrared photo detector which was read by the analog pin of the Arduino Uno. With this method, the micro-controller determined when the motor had completed one rotation, which was used as a check for the position of the monochromators.

The reflector sensor was used as a safety measure for the rotation of the monochromator. The sensor was located beneath one of the monochromators. The reflector sensor also consisted of an infrared LED light and infrared photo detector. However, instead of directly measuring the light from the LED, the photo detector measured how much of the light was reflected from the under surface of the monochromator. As the monochromator reached its limit of rotation, the under surface changed from opaque to reflective. This changed the amount of light received by the photo detector. The Arduino micro-controller then signaled to the monochromator motor to stop rotating. This was used as a safe guard to stop the monochromator motor from forcing the monochromators to rotate too far and break.

4 Summary

Absorption and PL was observed for magnetite iron oxide NPs, with an energy in agreement with expected values. The absorption and PL can be repeated at low-temperatures, with a range of 1.5 K to 300 K. The low-temperature experimental set up was created, and continued to be modified in response to the absorption peaks conflicting with the xenon lamp light source plasma lines. A double monochromator spectrofluorometer was also reconstructed, and rewired from an outdated electronic system to modern technology and computer interface. The reconstructed spectrofluorometer could be used to further characterize the optical properties of NPs. This system allows for simpler, quicker measurements with a narrower excitation and emitted light frequency selection. The spectrofluorometer will be available for optical measurements once the slit widths and rotation of the monochromators calibrated.

For future work, the NP thin films will be remade to allow for more accurate PL measurements. This could possibly be done using quartz cover slips versus glass. By recreating

thin films, the PL optical properties of magnetite iron oxide NP thin films could be determined. Additionally, low-temperature PL measurements could be taken to observe physical properties such as the Varshni shift of band gap energies. Temperature-dependent absorption and PL will also be taken of the Tb- and Eu-doped NPs. Finally, the magnetic properties of the excitons of the doped and undoped NPs will be examined using magnetic circular dichroism (MCD), which is a measure of the difference in absorption under left and right circularly polarized light.

5 References

[1] A. Schlegal, S.F. Alvarado, and P. Wachter, 1979. "Optical properties of magnetite (Fe_3O_4)", Solid State Physics. 12:1157-1164.

[2] M. Setvn, M. Wagner, M. Schmid, G.S. Parkinson, and U. Diebold, 2017. "Surface point defects on bulk oxides: atomically-resolved scanning probe microscopy", Chem. Soc. Rev, 46:1772-1784.

[3] H. Bin Na, K. Soo Kim, and L. Jung, 2007. "Development of a T1 Contrast Agent for Magnetic Resonance Imaging Using MnO Nanoparticles", Angewandte Chemie International, 46:1-6.

[4] D.L.J. Thorek, A.K. Chen, J. Czupryna, and A. Tsourkas, 2006. "Superparamagnetic Iron Oxide Nanoparticle Probes for Molecular Imaging", Annals of Biomedical Engineering, 34(1):23-38.

[5] K.P. Rice, S.E.Russek, R.H.Geiss, J.M.Shaw, R.J.Usselman, E.R.Evarts, T.J. Silva, H.T. Nembach, E.Arenholz, and Y.U.Idzerda, 2015. "Temperature-dependent structure of Tb-doped magnetite nanoparticles", Appl. Phys. Lett., 106,062409.

[6] W. Huan, C. Cheng, Y. Yang, H. Yuan, Y. Li, 2012. "A Study on the Magnetic and Photoluminescence Properties of Eu^{n+} and Sm^{3+} Doped Fe_3O_4 Nanoparticles", Journal of Nanoscience and Nanotechnology, 12:4621-4634.

[7] V.I. Klimov, *Nanocrystal Quantum Dots*, 2nd ed,. CRC Press, 2010.

[8] "Development of X-ray crystallography", publish.illinois.edu, 2014. https://publish.illinois.edu/x-raycrystallography/2014/12/18/introduction/

[9] V.P. Varshni, 1967. "Temperature dependence of the energy gap in semiconductors", Physica, 34:149-154.

[10]E. Hecht, *Optics*, 4th ed., Pearson, 2002.

[11]"Excitation of Photoluminescence", Caltech, https://ned.ipac.caltech.edu/level5/Sept03/Li/Li4.html

[12]A.C. Melissinos and J. Napolitan, *Experiments in Modern Physics*, 2nd ed., Academic Press, 2003.

[13]M.E. Sadat, M.K. Baghbador, A.W. Dunn, R.C. Ewing, J. Zhang, H. Xu, G.M. Pauletti, D.B. Mast, and D. Shi, 2014. "Photoluminescence and photothermal effect of Fe_3O_4 nanoparticles for medical imaging and therapy", Appl. Phys. Lett. 105, 091903.

[14]A. Najar, M. Shafaa, and D. Anjumb, 2017. "Synthesis, optical properties and residual strain effect of GaN nanowires generated via metal-assisted photochemical electroless etching", SRC Adv., 7:21697-21702.